



LAWRENCE  
LIVERMORE  
NATIONAL  
LABORATORY

# Neutron Production from Feedback Controlled Thermal Cycling of a Pyroelectric Crystal Stack

Vincent Tang, Glenn Meyer, Greg Schmid, Chris Spadaccini, Phil Kerr, Brian Rusnak, Steve Sampayan, Brian Naranjo, Seith Putterman

August 10, 2007

Review of Scientific Instruments

This document was prepared as an account of work sponsored by an agency of the United States Government. Neither the United States Government nor the University of California nor any of their employees, makes any warranty, express or implied, or assumes any legal liability or responsibility for the accuracy, completeness, or usefulness of any information, apparatus, product, or process disclosed, or represents that its use would not infringe privately owned rights. Reference herein to any specific commercial product, process, or service by trade name, trademark, manufacturer, or otherwise, does not necessarily constitute or imply its endorsement, recommendation, or favoring by the United States Government or the University of California. The views and opinions of authors expressed herein do not necessarily state or reflect those of the United States Government or the University of California, and shall not be used for advertising or product endorsement purposes.

This work was performed under the auspices of the U.S. Department of Energy by University of California, Lawrence Livermore National Laboratory under Contract W-7405-Eng-48.

## Neutron Production from Feedback Controlled Thermal Cycling of a Pyroelectric Crystal

V. Tang, G. Meyer, J. Morse, G. Schmid, C. Spadaccini, P. Kerr, B. Rusnak, and S. Sampayan, Lawrence Livermore National Laboratory, Livermore, Ca

B. Naranjo and S. Putterman, University of California at Los Angeles, Los Angeles, Ca

### Abstract

The LLNL Crystal Driven Neutron Source is operational and has produced record ion currents of  $\sim 10$  nA and neutron output of  $1.9 (\pm 0.3) \times 10^5$  per thermal cycle using a crystal heating rate of  $0.2$  °C/s from  $10$  °C to  $110$  °C. A  $3$  cm diameter by  $1$  cm thick  $\text{LiTaO}_3$  crystal with a socket secured field emitter tip is thermally cycled with feedback control for ionization and acceleration of deuterons onto a deuterated target to produce D-D fusion neutrons. The entire crystal and temperature system is mounted on a bellows which allows movement of the crystal along the beam axis and is completely contained on a single small vacuum flange. The modular crystal assembly permitted experimental flexibility. Operationally, flashover breakdowns along the side of the crystal and poor emitter tip characteristics can limit the neutron source. The experimental neutron results extend earlier published work by increasing the ion current and pulse length significantly to achieve a factor-of-two higher neutron output per thermal cycle. These findings are reviewed along with details of the instrument.

### I. Introduction

Recent work [1-3] has shown that electrostatic fields from the pyroelectric effect in specific crystals may be utilized to produce neutrons. Specifically, a  $\text{LiTaO}_3$  crystal with a nominal pyroelectric coefficient of  $K=190$   $\mu\text{C}/\text{m}^2\text{-}^\circ\text{C}$  [4] can be thermally cycled to produce charges and corresponding electrostatic fields which ionize and accelerate deuterons to  $\sim 100$ 's of keV. A tungsten tip field emitter on top of the crystal is typically used to enhance the electric field for ionization. The deuterium beam bombards a deuterated target and  $\sim 2.5$  MeV neutron emission occurs through the D-D fusion reaction. Figure 1 graphically illustrates the concept along with a typical Faraday cup setup for current measurement and neutron

production. The crystals after heating or cooling, and assuming no charge losses (i.e. ion emission, parasitic electrons, etc.), can reach a potential very roughly given by the 1-D estimate  $V=KA\Delta T/(C_{cr}+C_g)$  [5], where  $C_{cr}$  is the capacitance of the crystal and  $C_g$  is the stray capacitance in the gap between the front of the crystal and the target.  $A$  is the front surface area of the crystal, and  $\Delta T$  is the crystal temperature change. Practically, “pyrofusion” neutron sources could potentially be made very small with little high voltage equipment, and could for example, potentially be used for active interrogation of materials in the field.

In this work, we present first results from the LLNL Crystal Driven Neutron Source (CDNS) experiment based on the pyroelectric effect. The goal of the CDNS project is to extend the work done previously and ultimately raise the D-D neutron output from  $\sim 10^3$  n/s to  $\sim 10^6$  n/s by, for example, increasing the beam energy and current using different crystal configurations. Pulsed neutron emission is also desired. The beginning project objectives are to extend and reproduce the previous results from ref [1] using a more experimentally flexible crystal assembly and start to verify pyrofusion system models. To these objectives, the CDNS is operational and has produced record ion currents of  $\sim 10$  nA, neutron flat-tops  $\sim 170$  s long at  $924 \pm 141$  n/s, and total neutron output of  $1.9 (\pm 0.3) \times 10^5$  per thermal cycle. This is compared with neutron outputs of  $8.5 \times 10^4$  per cycle and  $5.9 \times 10^4$  per cycle from ref [1] and [3] with peak currents of  $\sim 4$  nA in ref [1]. The heightened neutron output and ion current is achieved by extending the thermal cycling range of the crystal from  $\sim 40$  °C to  $\sim 100$  °C in a controlled manner using a novel modular crystal assembly with feedback temperature control and configured for rapid changing of field emitters. Additionally, basic pyroelectric charge measurements were also performed and agreed with predictions. Lastly, it is found that the neutron emission and run reproducibility can be susceptible to HV breakdowns and field emitter tip condition.

## II. Experiment Setup

The present experimental setup primarily consists of a Kimball Physics 8.4” diameter spherical chamber with an array of modular beam and nuclear diagnostics, and a novel crystal assembly with a feedback controlled thermoelectric heater/cooler (TEC). Figure 2 illustrates the general setup with some of the diagnostics and provides a detailed view of the crystal assembly.

The modular crystal assembly consists of a crystal clamped onto the feedback controlled 39 W TEC which allows the crystal to be cycled from  $-20\text{ }^{\circ}\text{C}$  to  $120\text{ }^{\circ}\text{C}$  in a proscribed manner. The ability to proscribe temperature cycles in detail permit numerous possible crystal operating schemes. The entire crystal assembly is mounted onto a single  $2\frac{3}{4}$  vacuum flange with a bellows which allows the crystal to traverse along the beam axis. Relevant experimental parameters, such as target distance, can be changed easily in-situ. The crystal setup used for the neutron results in this work employ a 3 cm diameter by 1 cm thick  $\text{LiTaO}_3$  crystal with optical finish. The front and rear faces of the crystal is coated with a  $1000\text{ \AA}$  of platinum in lieu of the large copper plate used in ref [1] and ensures an even charge distribution. A smaller  $\sim 1$  cm diameter copper plate is mounted on the center of the crystal and has a single pin socket from a standard dual in-line package (DIP) mount for holding the 0.02" diameter shank of a tungsten tip field emitter with a  $1000\text{ \AA}$  radius apex. The tip apex is  $\sim 1.1$  cm above the face of the crystal but can be changed for different experiments. This socket approach allows rapid changing of field emitter tips for different experiments, and when tips are damaged. The base of the crystal is electrically and physically connected to a thin copper backplate via a low temperature indium-silver solder. There is a coat of Torrseal epoxy around the base of the crystal to ease the electric field stresses at the triple point, similar to the setup in ref [1]. The crystal with backplate is clamped to a copper heatsink with the TEC sandwiched in-between them using a Kel-F ring. Indium foil is compressed between the interfaces to ensure good thermal contact. The use of indium foil and mounting clamps instead of epoxies permit changing the setup quickly. The back of the crystal is grounded using thin indium strips which connects the crystal backplate to the heatsink and system ground electrically. The copper heatsink is cooled with circulating cooling water. A Labview program interfaces with an Alpha Omega 800 TEC feedback controller based on thermocouple readings from the center of the backplate and executes proscribed temperature ramps or flat-tops. Based on 1-D thermal modeling, the temperature gradient between the front and back of the crystal should be less than  $10\text{ }^{\circ}\text{C}$  for thermal ramps with rates of  $0.1\text{-}0.2\text{ }^{\circ}\text{C/s}$ . The crystal is aligned so that positive potentials are created when it is heated.

The experiment has several primary diagnostics. The first consists of a Faraday cup for ion beam measurement and has a fully deuterated erbium ( $\text{ErD}_2$ ) target mounted in it, similar to ref [1] and shown schematically in Figure 1. The target has a  $0.5 \mu\text{m}$  thick layer of erbium with an estimated deuterium loading between 1.95 and 2.05 based on analysis of other targets produced using the same setup and procedures [6]. Using an erbium density of  $9 \text{ gm/cc}$  and a deuterium loading of 2, the deuterium number density of the deuterated erbium film is  $6.5 \times 10^{22}/\text{cc}$ . The cup or target plate is biased at 54V to capture secondary electrons [7] and is 0.8 cm behind a grounded mesh with  $\sim 85\%$  transparency. Almost all of the secondary electrons are expected to have energies noticeably lower than the bias. The current from the target is recorded using a Keithley 6514 electrometer. A  $2'' \times 2''$  Ortec NaI detector mounted on a  $2 \frac{3}{4}''$  window provides an indirect voltage measurement by detecting the end point of the bremsstrahlung spectrum from backstreaming or stray electrons. Neutron emission is recorded through a  $14 \times 17''$  long  $^3\text{He}$  detector tube array covered with  $1.5''$  thick polyethylene moderator. The array is essentially insensitive to gammas and has a calibrated 2.5 MeV neutron detection efficiency of  $3 (\pm 0.45) \times 10^{-3}$  for the experiment. The calibration was done with both a known D-D neutron tube and californium-252 source, and accounts for the experiment geometry along with the slight anisotropy of the D-D neutron emission. A set of firewire CCD cameras are used to observe breakdowns and for in-situ examination of the field emitter tip.

### III. Operating Results

The first set of experiments simply involved a direct charge measurement in air (1 atm) using the Keithley 6514 electrometer. The Coulomb probe was placed in direct contact with the front of a crystal which had a 2.8 cm diameter copper plate mounted to its face using vacuum silver epoxy instead of the more complex platinum coating described in Section II. The backplate in this preliminary setup was also mounted with the same epoxy. The TEC was ramped as quickly as possible from room temperature to a specific set point, and ramped back down after thermal equilibrium was reached. The detected charge was  $>90\%$  of the expected value, based on  $190 \mu\text{C}/\text{m}^2\text{-}^\circ\text{C}$ . Figure 3 plots the measurement. The finite rise time of the curves is due to the thermal diffusion time of the crystal, estimated as  $\sim 100 \text{ s}$ .

Experiments to produce beams and neutrons followed the basic charge experiments. Figure 4 plots the relevant parameters for an experiment using the assembly described in Section II. The crystal temperature was heated from 10 °C to 110 °C at 0.2 °C/s and held at 110 °C for 600 s, then cooled back down to 10 °C. The data after  $t=600$  s is not shown in the figure since no ion current was detected afterwards. The proscribed feedback controlled temperatures and measured rear crystal temperatures essentially matched each other with little overshoot, undershoot, or lag. A static fill of  $\sim 3$  mTorr  $D_2$  gas was used. The emitter tip apex was  $\sim 2.4$  cm away from the grounded mesh of the Faraday cup, and  $\sim 3.2$  cm away from the biased target or current collector. The height of the tip apex above the crystal was again  $\sim 1.1$  cm. As the beam current rose, the bremsstrahlung spectrum from the NaI detector indicated beam energies of  $\sim 80$  keV, resulting in a noticeable neutron emission flat-top from  $t=280$  to 450 s at an average rate of  $924 \pm 141$  n/s after background subtraction and accounting for the detector efficiency of  $3 (\pm 0.45) \times 10^{-3}$ . A background value of 1.1 n/s was used. This background is theorized to stem from cosmic-ray interactions. The total number of measured neutrons from  $t=0$  to  $t=600$  s, after background subtraction, was  $578 \pm 43$ . This gives a total source neutron output per thermal cycle of  $1.9 (\pm 0.3) \times 10^5$  neutrons. Assuming a mesh transparency of  $\sim 85\%$ , a peak current of  $\sim 9.5$  nA was recorded for this run. These results extend the beam current and neutron output of previous work by a factor-of-two.

For comparison, Figure 5 plots another  $\sim 3$  mTorr  $D_2$  run using the preliminary crystal setup described in the charge measurement experiment. The field emitter tip apex in this case was only  $\sim 1.4$  cm from the grounded mesh. The tip was not mounted using a socket and had an apex  $\sim 0.4$  cm above the crystal. A slower ramp rate and shorter temperature swing was also used. This run resulted in greater measured current,  $\sim 10$  nA, but lower beam energies at  $\sim 35$ -40 keV. Very few neutrons above background were detected for this run due to the low beam energy.

The enhanced electric field at the tip apex for both of the above runs should have been greater than  $\sim 100$  MV/cm, based on field enhancement factors extrapolated and estimated from ref [8]. The measured neutron emission rate and beam energies for the first run indicate that the beam was dominantly made of  $D^+$ , and not  $D_2^+$ ; this concurs with beam-target simulations using stopping powers from SRIM [9] and

fusion cross-sections from ENDL99 evaluations which indicates a neutron output of 850 n/s for an 8 nA 80 keV  $D^+$  beam impinging on the fully deuterated erbium target. The slight increase in recorded current for the second run could be due to higher collection efficiency, since the beams are expected to be divergent. The lower potential or beam energy could be partly due to an increase in stray capacitance, or  $C_g$ , as the crystal is closer to the ground mesh, and also charge neutralization due to any electrons pulled from the mesh or target. During the cooling portion of the thermal cycle for the numerous runs performed, electron emission was seen as expected. A systems modeling effort is underway to simulate and understand these experimental data.

Reproducibility of runs is complicated by changing field emitter tip condition and high voltage breakdowns. Each time a breakdown occurs, the beam collapses and the effective available charge on the crystal is changed. Breakdowns occur easily as the electric fields between the front and back of the crystal are on the order of  $\sim 100$  kV/cm, easily exceeding the typical DC surface breakdown fields of  $\sim 20$  kV/cm [10]. Figure 6 shows a breakdown captured by an Imaging Source color CCD firewire camera, and also another run where an arc occurred at the tip apex. The breakdowns typically occur as a flashover on the side of the crystal, as shown by Figure 6a. Emitter tip condition affects the ion current noticeably; runs with damaged tips like the one in Figure 6b resulted in significantly less or zero ion current. Typically, depending on experimental conditions, maximum ion currents in the  $\sim 0.5$  to  $\sim 10$  nA range were achieved.

#### **IV. Conclusion**

We have shown a factor-of-two increase in ion current and neutron output in the LLNL CDNS experiment over previous pyrofusion work. This was achieved by increasing the temperature swing of the pyroelectric crystal in a controlled feedback manner using a novel crystal assembly. The incorporation of feedback temperature control, socket mounts for rapid changing of field emitters, and the ability of the assembly to traverse the beam axis permits maximum experimental flexibility. In general, flashover breakdowns and poor emitter tip conditions were found to affect the reliability of the source. We are now working on applying high voltage engineering methods such as corona rings, and accelerator techniques to reliably

achieve greater voltage and beam currents in order to increase the D-D neutron emission from  $\sim 10^3$  n/s to  $\sim 10^6$  n/s.

### Acknowledgements

The authors acknowledge fruitful discussions with S. Falabella, J. Harris, L. Wang, G. Guethlein, and G. Caporaso at LLNL. This research is supported by the Defense Sciences Office of the Defense Advanced Research Projects Agency (DARPA) and the Laboratory Directed Research and Development (LDRD) Program at LLNL. Work is performed under the auspices of the US Dept. of Energy by LLNL under contract No. W-7405-Eng-48.

### References

- [1] B. Naranjo, J. Gimzewski, and S. Putterman, *Nature* **434**, 1115 (2005).
- [2] J. Geuther, Y. Danon, and F. Saglime, *Phy. Rev. Lett.* **96**, 054803 (2006).
- [3] J. Geuther and Y. Danon, *Appl. Phys. Lett.* **90**, 174103 (2007).
- [4] A. M. Glass, *Phy. Rev.* **172**, 564 (1968).
- [5] G. Rosenman, D. Shur, Ya. E. Krasik, and A. Dunaevsky, *J. Appl. Phys.* **88**, 6109 (2000).
- [6] Private conversation, Dr. Thomas Venhaus, LANL, 2007.
- [7] E. J. Sternglass, *Phy. Rev.* **108**, 1 (1957).
- [8] C. J. Edgcombe and U. Valdrè, *J. Microscopy* **203**, 188 (2001).
- [9] J. F. Ziegler, J. P. Biersack, and U. Littmark, *The Stopping and Range of Ions in Matter* (Pergamon, New York, 2003).
- [10] S. Humphries, *Principles of Charged Particle Acceleration* (Wiley and Sons, 1986).

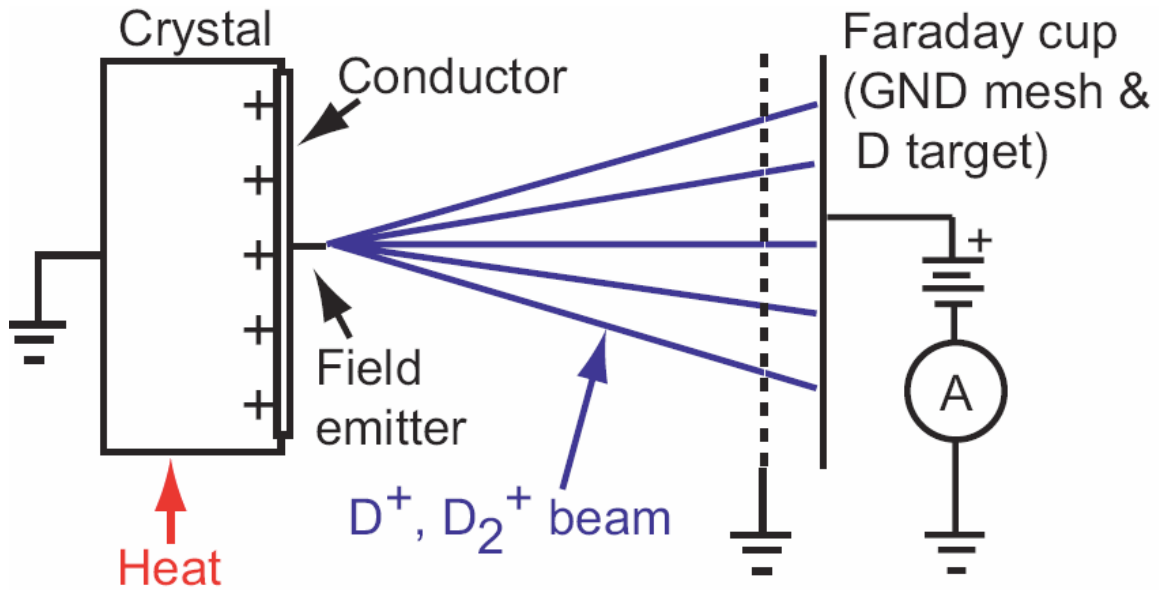


Figure 1) Schematic of the pyrofusion concept and a typical Faraday cup-target setup for ion current measurement [1]. The current collector or target plate behind the grounded mesh is loaded with deuterium for D-D fusion and connected to an ammeter for current measurement. The collector is operated with a positive bias to prevent the escape of secondary electrons [7].

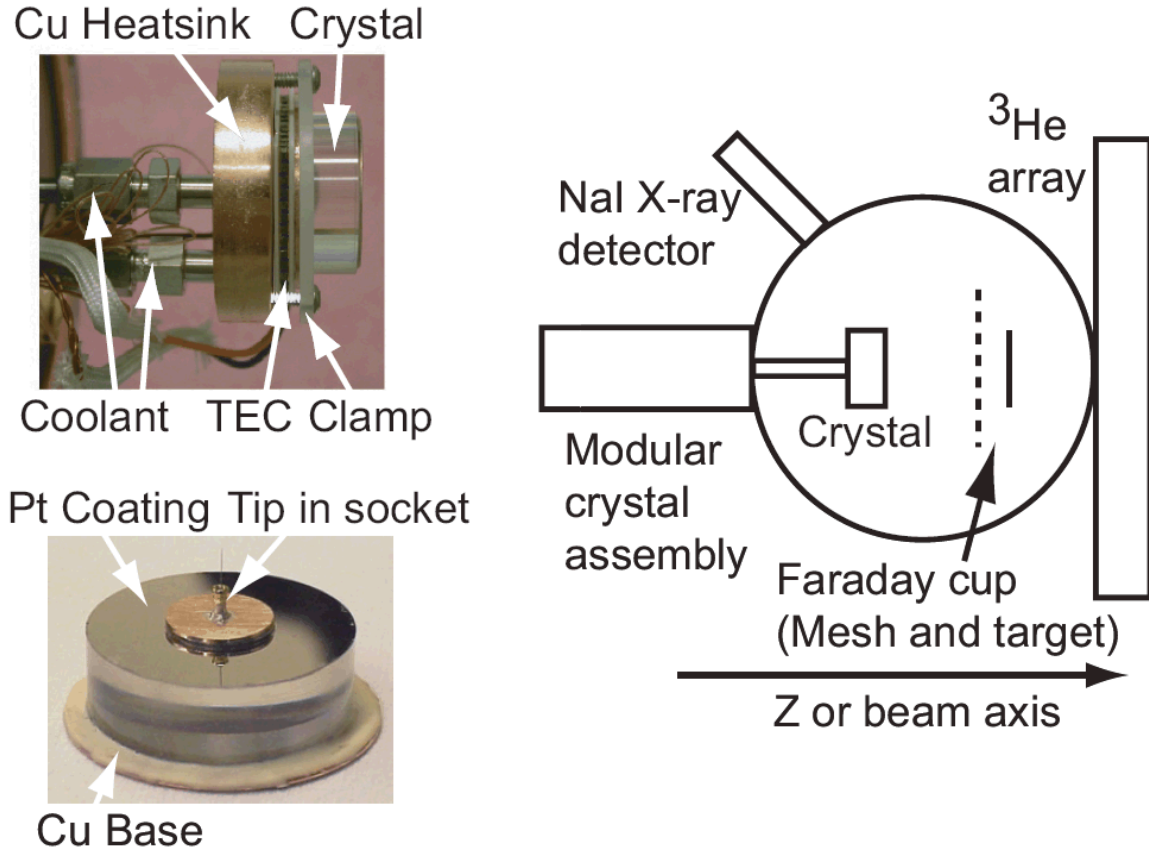


Figure 2) Schematic of the CDNS with close-up views of the modular crystal assembly and one of the crystals. The crystal can be moved back and forward along the beam axis. The thermocouple for feedback control is sandwiched between the TEC and the copper backplate on the rear of the crystal. A groove cut into the backplate allows the thermocouple to be sandwiched snugly without causing a gap between the TEC and the backplate.

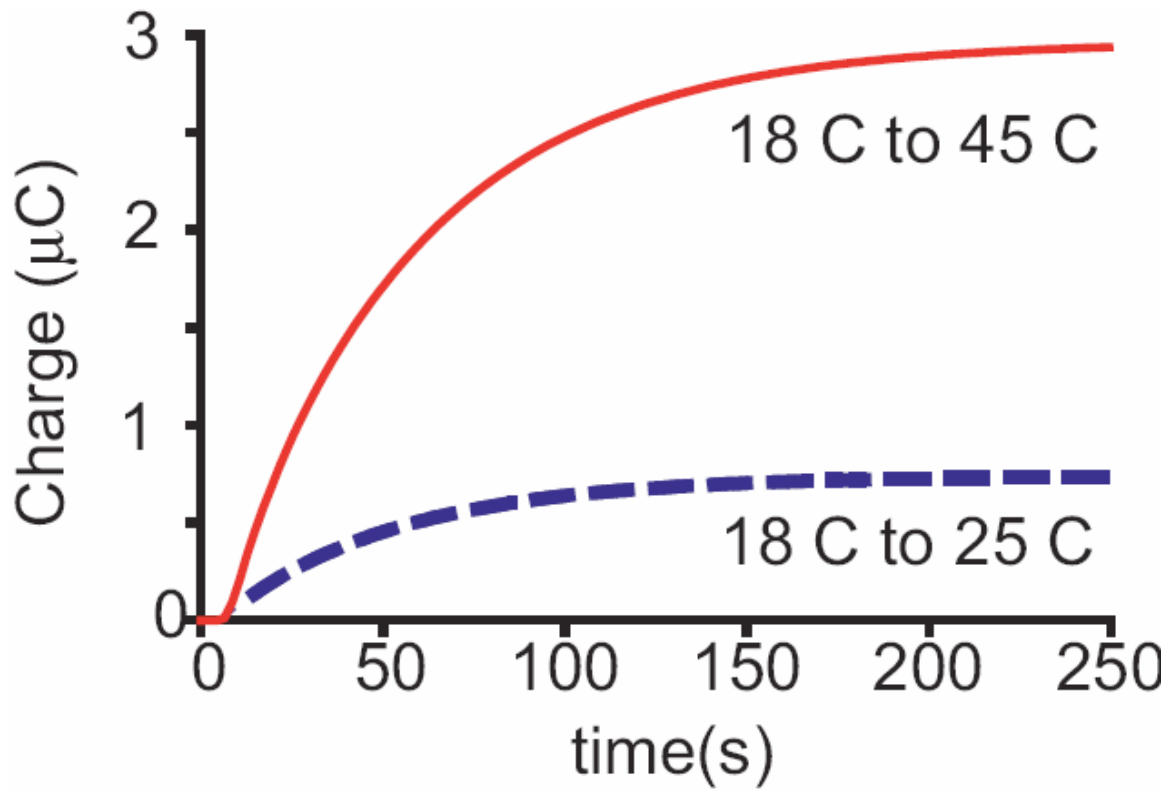


Figure 3) Direct charge measurements in air (1 atm) for different temperature ramps.

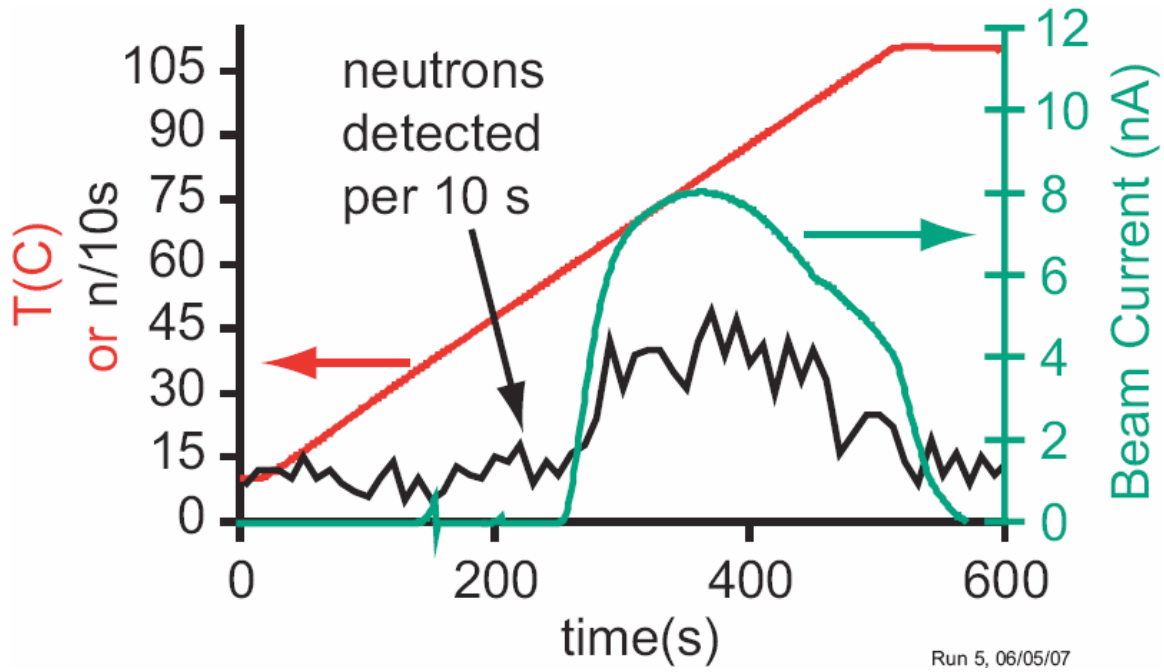


Figure 4) Measured beam current (right), detected neutrons per 10 s (left), and rear crystal temperature (left). The proscribed temperatures essentially match the measurements and hence are not shown for clarity. The neutron flat-top between  $t=280-450$  s has an average source emission rate of  $924 \pm 141$  n/s based on a detector efficiency of 0.3%. A total of  $1.9 (\pm 0.3) \times 10^5$  neutrons was produced by the source from  $t=0$  to  $t=600$  s. A background neutron rate of 1.1 n/s was used for background subtraction.

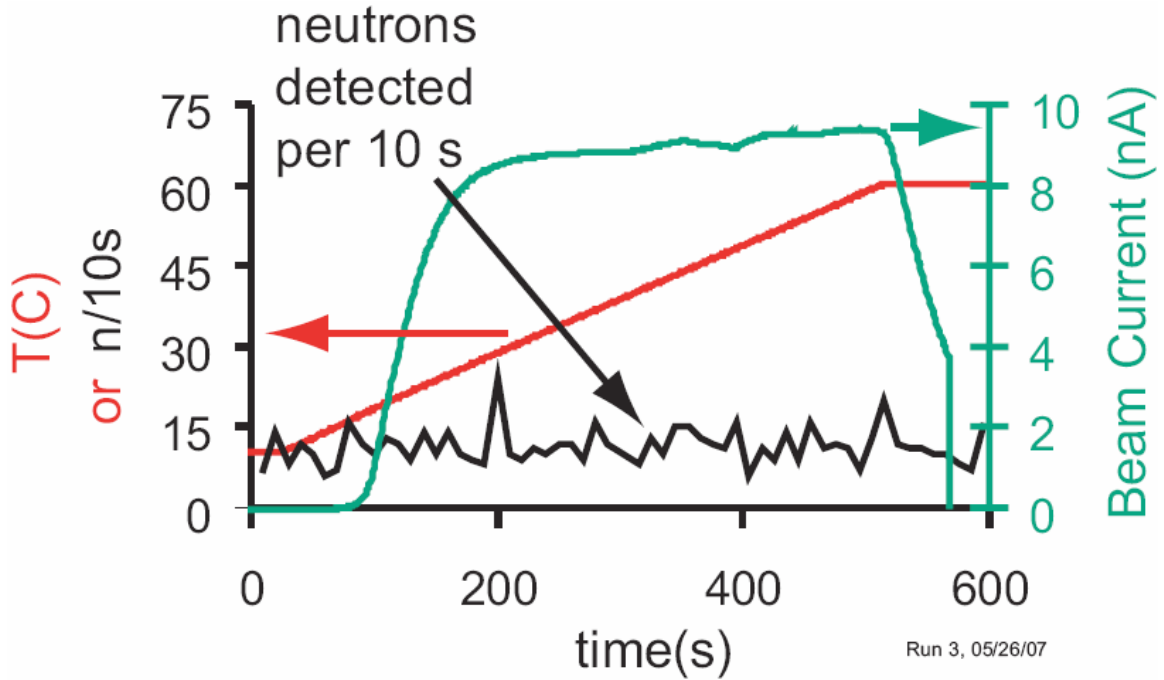


Figure 5) Measured beam current (right), detected neutrons per 10 s (left), and rear crystal temperature (left) for highest measured current run. The beam energy was only ~35-40 keV. The beam collapsed at ~575 s due to breakdown. Very few neutrons above background were detected for this run due to the low beam energy.

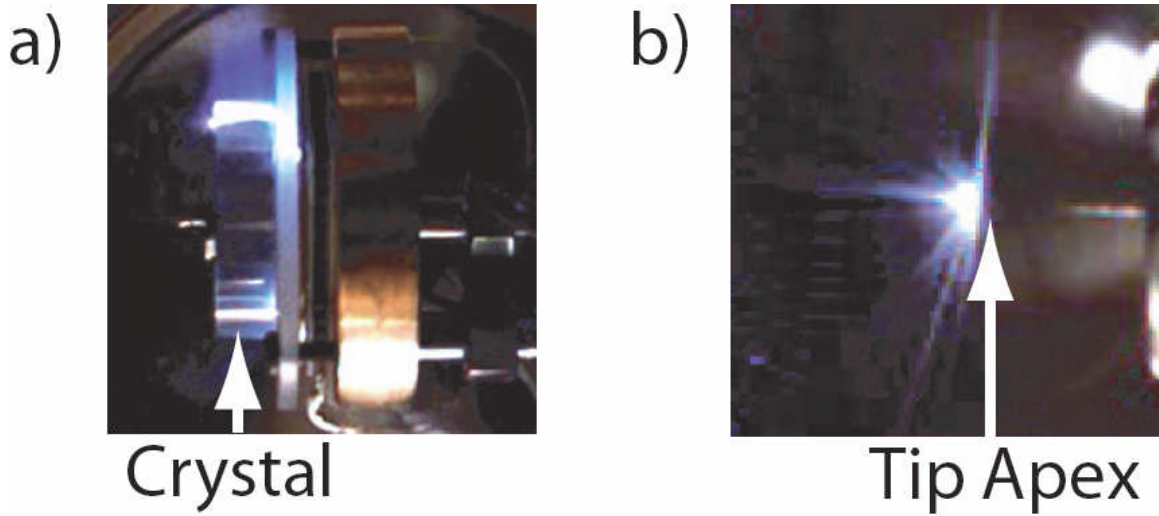


Figure 6a) Typical surface flashover breakdown on crystal side. 6b) Arcing to field emitter tip; the 0.02" diameter shank is visible but the tungsten tip and its apex is not due to its small radius. The socket mount design shown here is slightly different than the one described in Section II.